applied sciences

MDPI

Article

# Surface Erosion Analysis for Thermal Insulation Materials of Graphite and Carbon–Carbon Composite

**Youngin Kim [1] and Jeongho Cho [2,*]**

[1] School of Comprehensive Aviation, Hanseo University, Taean 32158, Korea
[2] Department of Electrical Engineering, Soonchunhyang University, Asan 31538, Korea
* Correspondence: jcho@sch.ac.kr; Tel.: +82-41-530-4960

Received: 17 July 2019; Accepted: 10 August 2019; Published: 13 August 2019


**Abstract:** A rocket uses fuel and oxidizers to generate propulsion by combustion and ejection, and is used for space exploration aircrafts, weapons, and satellite launches. In particular, the nozzle generating thrust of solid-propellant rockets is exposed to a high-temperature and high-pressure environment with erosion occurring from the combustion gas. When erosion occurs on the nozzle throat of such a rocket, it has a great impact on the flight performance such as reaching distance and flight speed. Many studies have been conducted to characterize erosion based on the thermochemical erosion model, since it has become important to choose nozzle materials suitable for such environments having robustness against combustion gasses of high temperature and high pressure. However, there is a limit to fully analyze the erosion characteristics only by the thermochemical erosion model. In this paper, we thus consider the mechanical erosion model with the thermochemical model for better understanding of erosion characteristics and investigate the thermochemical and mechanical erosion characteristics of nozzle throat heat-resistant materials made of graphite and carbon–carbon composites; the main factors affecting erosion are discussed by comparing the results of the experimental and theoretical models.

**Keywords:** carbon–carbon composites; erosion; graphite; porosity; rocket nozzle throat

## 1. Introduction

A rocket is a device that generates thrust through action and reaction forces. It uses fuel and oxidants to generate propulsion by combustion and emissions, and is mainly used for space exploration aircrafts, weapons and satellite launches. Examples include liquid-propellant, solid-propellant, nuclear propulsion, and laser propulsion rockets. Among them, solid-propellant rockets consist of a motor case, igniter, propellant, nozzle, insulator, and control and drive device. The nozzle is a very important component that generates thrust. However, since the nozzle is burnt in a high-temperature/high-pressure environment, it cannot be cooled, unlike the liquid-propellant rocket that circulates fuel around the nozzle. As a result, solid-propellant rockets experience erosion due to combustion gas [1].

The nozzle throat of a rocket is a portion where the gas pressure and density are comparatively high, and the velocity of the gas becomes the speed of sound and the amount of heat transferred to the nozzle wall is significant. When erosion occurs on the nozzle throat of such a rocket, it affects the reaching height, reaching distance, and flight speed [1]. Therefore, one of the most important issues in nozzle design is to select or develop materials suitable for such environments that have durability against combustion gases of high temperature and pressure. Bulk-type graphite and carbon–carbon (C–C) composite materials have been mainly used for solid-propellant rocket nozzles. In particular, C–C composites are made by laminating multiple layers of carbon fibers and have recently been used because of their relatively strong thermal shock and mechanical strength compared to graphite.

An oxy-acetylene torch test has been used for basic research and evaluation of erosion materials [2]. Many studies have been performed by Bianchi and Nasuti and other researchers to characterize erosion based on the thermochemical erosion model previously presented by Kuo and Keswani [3,4]. This model consists of a chemical-controlled recession process and a diffusion-controlled recession process. However, the thermochemical erosion model alone has limits in fully understanding the erosion characteristics. In addition, there are few analyses of the improved erosion characteristics using a mechanical erosion model, including the friction factor, porosity, and characteristic exhaust velocity proposed by Gowariker [5] in the thermochemical erosion model for graphite and C–C composite materials.

In this study, the mechanical erosion model is considered with the thermochemical model for better analysis of erosion characteristics. The parameters required for the thermochemical erosion model of graphite and C–C composite materials were experimentally measured through the development of the erosion experimental system, and the main factors influencing the erosion were compared with the model. Additionally, the characteristics of mechanical erosion of graphite and C–C composite materials were investigated experimentally; more accurate erosion was predicted, and major factors influencing the mechanical erosion were analyzed.

## 2. Materials and Methods

### *2.1. Theoretical Erosion Model*

Figure 1 shows the physical and chemical processes of rocket nozzle erosion in which convection and radiation heat transfer occurs through combustion gas, and conduction heat transfer occurs in the nozzle. A heterogeneous reaction occurs at the nozzle surface and gas-phase chemical species diffusion, pyrolysis, and evaporation occur. Finally, by combustion gas flow, surface deviation occurs and the nozzle surface is eroded. Thermochemical erosion can be divided into a chemical-controlled recession process and a diffusion-controlled recession process; the effect depends on the surface temperature [6].

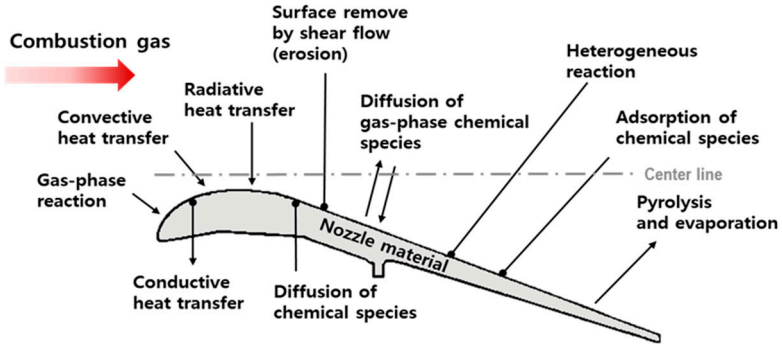


**Figure 1.** Physical and chemical processes associated with rocket nozzle erosion.

Surface temperature, surface pressure, reactant and product concentration, and density are the most influential factors for thermochemical erosion. Density of material has a large effect on erosion, and the higher the density, the more resistant to erosion. As the combustion chamber pressure increases, the density of the gas increases and the erosion increases [7]. Additionally, the higher the temperature, the greater the effect of erosion, which is due more to the diffusion-controlled recession process than the chemical-controlled recession process [4]. In the effects of chemical species, erosion is proportional to the concentration of $H_2O$, $CO_2$, and OH, and inversely proportional to the concentration of $H_2$ by the reaction of $H_2O$ and $CO_2$, which are the main causes of erosion, wherein the C–C composite or graphite produce CO [8,9]. Mechanical erosion is dominated mainly by the characteristic exhaust velocity, the friction coefficient and porosity. The characteristic exhaust velocity is a measure of combustion performance and depends on chamber pressure, nozzle cross-sectional area, and mass flow rate [10].

The coefficient of friction is the shear stress at the surface and the porosity is the measure of the structural resistance [6].

The chemical-controlled recession process in the thermochemical erosion can be described in Equation (1) as a heterogeneous chemical reaction, where $H_2O$, $CO_2$, and OH are the main oxide and $H_2$, CO, and H are the main products [11].

$$\begin{array}{c} C_s + H_2O \rightarrow CO + H_2 \\ C_s + CO_2 \rightarrow 2CO \\ C_s + OH \rightarrow CO + H \end{array} \quad (1)$$

Here, $C_s$ is the carbon of the material surface and other species such as O, $O_2$, and NO are ignored because they have little effect on the chemical reaction. The reaction rate constant ($K_i$) for species i is expressed by the Arrhenius equation as follows:

$$K_i = A_{s,i} T_i^{\beta} \exp\left(-\frac{E_{a,s,i}}{R_u T_s}\right) \quad (2)$$

Here, A is the pre-exponential factor, β is the temperature exponent, E is the activation energy, $R_u$ is the universal gas constant, and T is the surface temperature. The chemical dominant erosion rate at the surface is expressed as Equation (3) [12].

$$\dot{r}_{c,ch} = \sum K_i P_i^{n_i} / \rho_c \quad (3)$$

Here, $P_i$ is the pressure of i chemical species and the reaction rate data for the heterogeneous reaction are shown in Table 1 [13]. $\rho_c$ is density of graphite or carbon–carbon composite.

**Table 1.** Kinetic data for heterogeneous reactions.

| Surface Reactions | $A_i$ | $E_i$ (Kcal/mol) | $\beta$ | $N$ | Remarks |
|---|---|---|---|---|---|
| $C_S + H_2O \rightarrow CO + H_2$ | $4.8 \times 10^5$ (kg/m$^2$ s atm$^{0.5}$) | 68.8 | 0.0 | 0.5 | |
| $C_S + CO_2 \rightarrow 2CO$ | $9.0 \times 10^3$ (kg/m$^2$ s atm$^{0.5}$) | 68.1 | 0.0 | 0.5 | |
| $C_S + OH \rightarrow CO + H$ | $3.61 \times 10^2$ (kg K$^{0.5}$/m$^2$ s atm) | 0.0 | −0.5 | 1.0 | MOS |
| | 100 (kg K$^{0.5}$/m$^2$ s atm) | 0.0 | −0.62 | 1.0 | MMOS |

The diffusion-controlled recession process in thermochemical erosion can be expressed as a surface mass balance (SMB) [14] at the solid–gas interface, as illustrated in Figure 2 and Equation (4).

$$\left(\overline{\rho}\widetilde{v}\widetilde{Y}_i\right)_g + \left(\overline{\rho} D \frac{\partial \widetilde{Y}_i}{\partial r}\right)_g = \dot{\omega}_i - \frac{1}{A}\frac{d}{dt}\iint_{S_1} \rho_i' ds + \rho_c \dot{r}_c \widetilde{Y}_i \quad (4)$$

The left side of Equation (4) indicates the convective mass flux and the diffusion mass flux of the species i, and the right side is the rate of generation of species i, the rate of mass accumulation of species i, and mass flux of species i. Here, $S_1$ is the interfacial surface area, Y is the mass fraction, A is the area, ρ is the density, and $\dot{r}_c$ is the erosion rate. When the temperature is high at the solid-gas interface, the reactant reacts with carbon, resulting in a very low concentration. The mass fraction can be assumed to have no accumulation. So $\left(\widetilde{Y}_i\right) \cong 0$ and Equation (4) is reformulated as follows:

$$\dot{\omega}_i + \rho_c \dot{r}_c \widetilde{Y}_i = 0 \quad (5)$$

The reaction between the reactant $B_i$ and graphite or the C–C composite $C_s$ is as follows:

$$\nu_{c,i} C_s + \nu_{Bi} B_i = \sum_j \nu_j Prod_j \quad (6)$$

Consequently, the diffusion-controlled recession rate ($\dot{r}_{c,d}$) on the surface of graphite or the C–C composite can be expressed as Equation (7) based on Equations (5) and (6).

$$\dot{r}_{c,d} = \frac{1}{\rho_c} \sum_i \dot{\omega}_i \frac{\nu_{c,i}}{\nu_{B,i}} \frac{MW_C}{MW_{B_i}} \tag{7}$$

Here, MW is the molecular weight and ν is the stoichiometric coefficient.

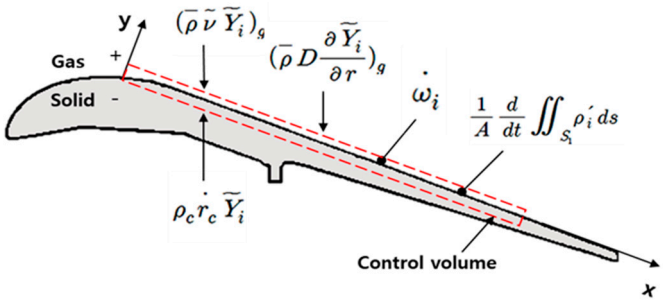


**Figure 2.** Surface mass balance at solid-gas interface.

The mechanical erosion model is expressed by the porosity of the material, the characteristic exhaust velocity, and the experimental constant. The Hopf equation is expressed by the relationship between the friction factor and surface roughness as Equation (8).

$$f = C_1 e^{C_2} \tag{8}$$

Here, $f$ is the friction coefficient, C is a constant, and e is a dimensionless constant. Equation (8) is again given by Equation (9), taking into account of the porosity that is the measure of the structural resistance of the material, where $a_1$ is a constant and $P$ is the porosity.

$$f = a_1 (\log P)^2 \tag{9}$$

The shear flow of the gas causes shear stress in the wall, and mechanical erosion has a linear relationship with shear stress. The mechanical erosion rate ($\dot{r}_m$) is expressed as Equation (10), a function of the characteristic exhaust velocity ($c^*$) and friction coefficient ($f$) related to the shear stress, and is a constant.

$$\dot{r}_m = a_2 c^* f \tag{10}$$

Substituting Equation (9) into Equation (10), the mechanical erosion rate is summarized as $\dot{r}_m = ac^*(\log P)^2$ by the relationship between the porosity and characteristic exhaust velocity, where α is the final constant [5]. The total erosion rate is obtained using the harmonic mean for thermochemical chemical-controlled recession rate ($\dot{r}_{c,ch}$), thermochemical diffusion-controlled recession rate ($\dot{r}_{c,d}$), and mechanical erosion rate ($\dot{r}_m$). The harmonic mean is commonly used to obtain the average of the values with the same relative ratio as the unit [15], and to obtain the average of the change rates, as follows:

$$\dot{r}_{\text{total erosion}} = \frac{3}{\left(\frac{1}{\dot{r}_{c,\,ch}} + \frac{1}{\dot{r}_{c,d}} + \frac{1}{\dot{r}_m}\right)} \tag{11}$$

## 2.2. Design of Experiments

An oxy-acetylene torch test setup was used for erosion experiments. The equipment had the disadvantage of a low-calorie application and a low exposed surface but was still overall advantageous for evaluating the erosion characteristics because the experiment is convenient, simple and fast [16]. The test apparatus, shown in Figure 3, consists of an oxygen–acetylene control unit, a data measuring

unit, a data collecting and storing unit, and a specimen-fixing unit. The oxygen–acetylene control controls the flow rate, pressure, mixing ratio and time of oxygen and acetylene. A torch (Victor model 315FC) and tip (Type 4, No. 7) were used [17,18]. In addition, the correct operation time was set and controlled using an auto ignition device, a timer, and a solenoid valve. The pressure and temperature were measured using a pressure transducer (Dacell CMM-50K) and a thermocouple (K-type).

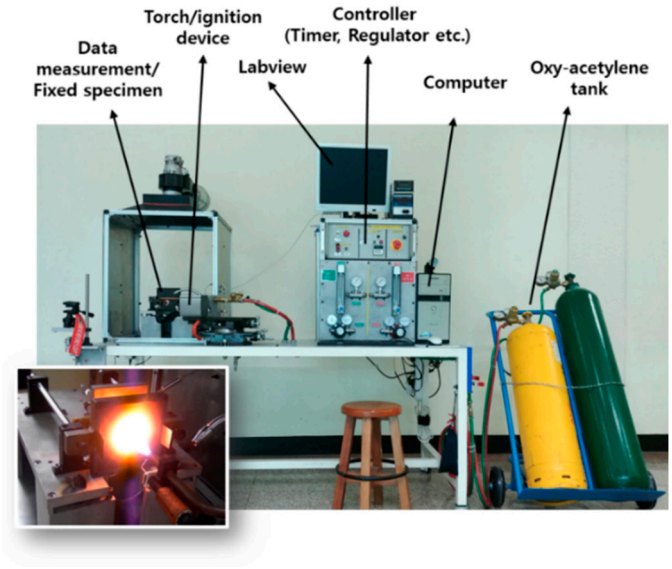


**Figure 3.** Oxy-acetylene torch test equipment.

The surface temperature was measured using an infrared thermometer (CHINO IR-AH) [19]. Data collection and storage were performed using the NI USB-6009 [20] and LabVIEW software. The pressure gauge was DN-50W, and the thermometer was KN-2000W. The cooling method was air, and compressed air was applied to the specimen fixing part, moving shaft, and sensor contact part to prevent equipment breakage and error due to the high temperatures. Figure 4 is a configuration diagram of the testing apparatus.

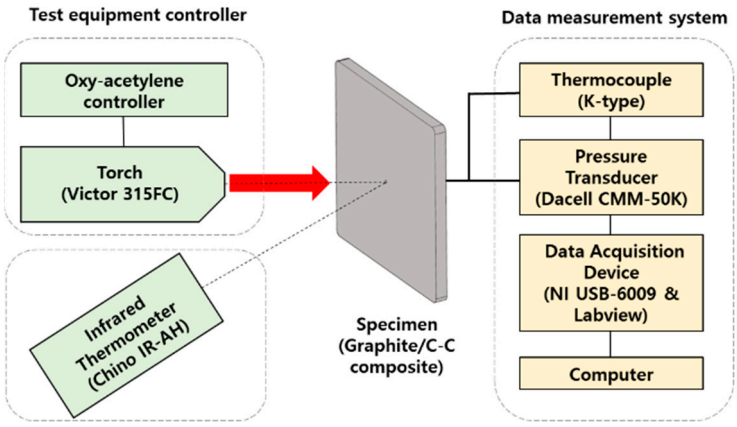


**Figure 4.** Schematic diagram of oxy-acetylene torch test equipment.

The size of the heat-resistant material specimens was 100.5 mm × 100.5 mm and 6.5 mm (thickness). The graphite used in the experiment was Grade 6520 of Mersen, R4340 of SGL, EX60 and EX70 of IBIDEN and the composite material was a custom-made 3D C–C composite. The density and porosity of the graphite and C–C composite are shown in Table 2. The oxygen and acetylene pressures were set to 0.12 MPa and 0.02 MPa, respectively. The flame was generated with a neutral flame with a 1:1 oxygen-acetylene ratio and the distance between the specimen and torch was set at 60 mm. The erosion

test duration was set to 120 s and the pressure applied to the specimen was measured in real time using the NI USB-6009 and LabVIEW, as described in Figure 4. Additionally, the surface temperature was measured using a radial thermometer from the front. Figure 5 shows the test results after 5, 40, and 100 s in the erosion test procedure for the 3D C–C composite specimen. The results are shown after 120 s, the end of the experiment. Cooling of the experimental apparatus was directed by air intensity so as not to affect the experiment.

**Table 2.** Density and porosity of the graphite and C–C composite.

| | Graphite | | | | C–C |
|---|---|---|---|---|---|
| | **G6520** | **R4340** | **EX60** | **EX70** | **3D** |
| Density ($kg/m^3$) | 1750 | 1770 | 1800 | 1850 | 1700 |
| Porosity (%) | 17 | 15 | 14 | 10 | 12 |

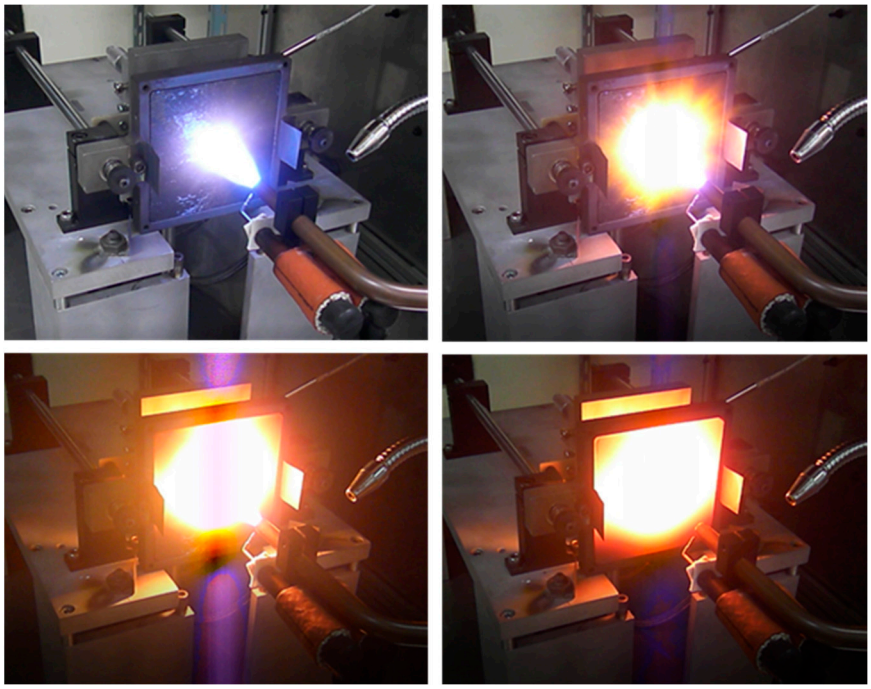

**Figure 5.** Erosion test results for the 3D C–C composite specimen after 5 s (**upper left**), 40 s (**upper right**), 100 s (**lower left**), and 120 s (**lower right**).

## 3. Experimental Results and Discussion

Figure 6 shows the erosion surface of five specimens, Graphite R4340, Graphite G6520, Graphite EX60, Graphite EX70, and 3D C–C composite, after the flame was injected for 120 s. The upper right picture in each figure is the one before the flame was applied to the specimen. In the case of graphite material, erosion occurred most in the center of the flame, and the white dot in the figure shows the surface groove due to erosion. The roughness of the specimen was increased due to the surface groove toward the center of the specimen. In the C–C composite material, the surface groove was larger than that of graphite as the matrix was burned and absent, and the fiber-reinforced composite material under the laminate was exposed due to erosion, appearing as a circular pattern. It was confirmed that five fibers were exposed by each 90° downward directions, but they were resistant to surface erosion while the matrix was removed.

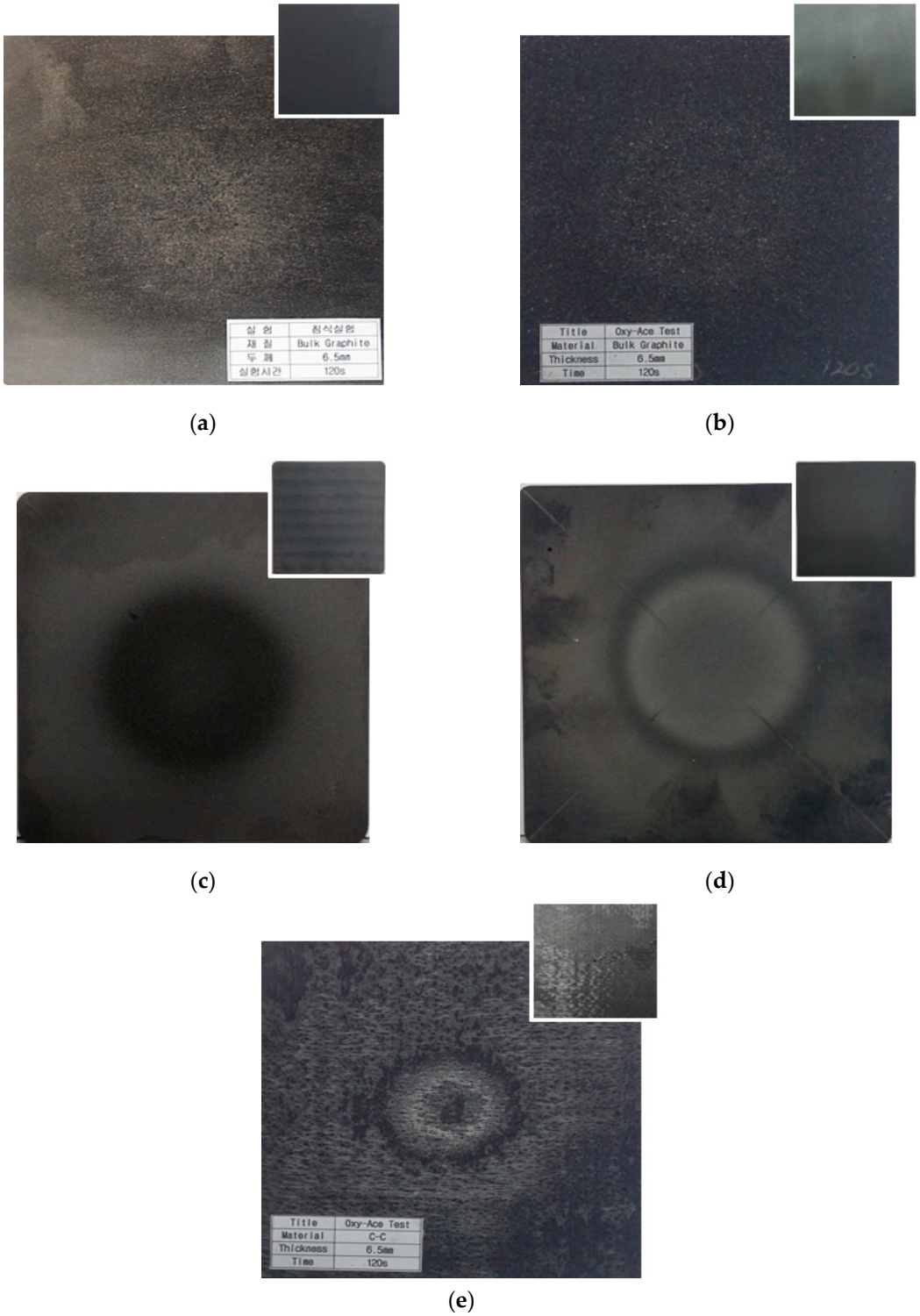


**Figure 6.** The eroded surface of (**a**) Graphite R4340, (**b**) Graphite G6520, (**c**) Graphite EX60, (**d**) Graphite EX70, (**e**) 3D C–C composite.

Figure 7 is the erosion test of Graphite G6520, and the dotted circle is a representation of the deviations of surface particles. The erosion intermittently occurred at the beginning of the experiment, but surface particles at high temperature in red started to be released at 1000 °C after 35 s, and the particles changed in all directions as time passed. In the case of the C–C composite material, the change in surface particles was observed after 20 s when the surface temperature reached 1000 °C. These surface

particle changes are erosion phenomena and the released particles are in the form of grooves on the surface.

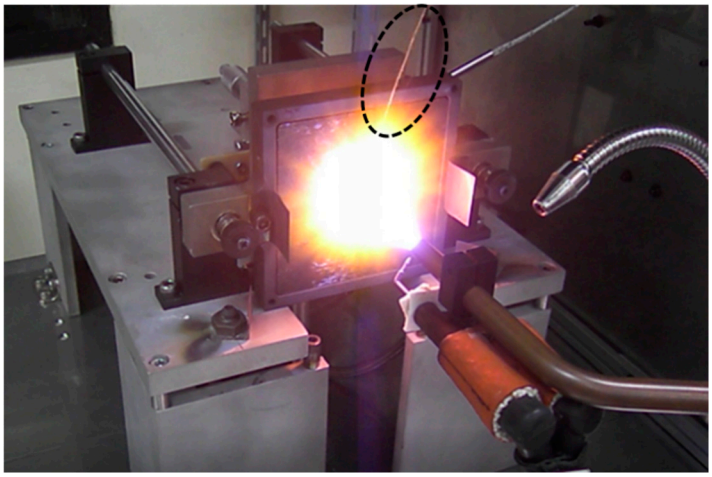

**Figure 7.** Surface particle changes of 3D C–C composite.

The surface temperatures of the graphite and C–C composite specimens were measured to investigate the characteristics of the above described particle surface change. As shown in Figure 8, the 3D C–C composite (thermal conductivity of 18 W/m K) reached a high temperature faster than Graphite G6520 (thermal conductivity of 160 W/m K).

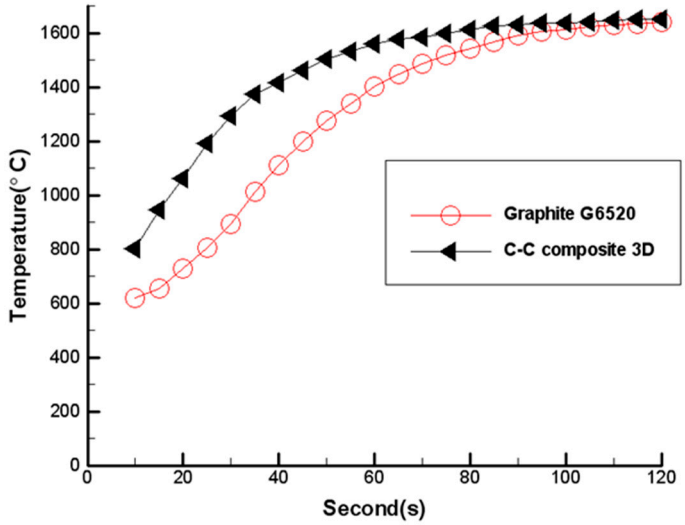


**Figure 8.** Comparison of surface temperature of Graphite G6520 and the 3D C–C composite.

The amount of erosion and erosion rate for each material for the erosion test conducted for 120 s are shown in Table 3, and the erosion cross section for each material is shown in Figure 9. To compare the measured erosion rates with the theoretical values, the thermochemical erosion rate ($\dot{r}_{ch}$) described in Table 4 was calculated using the chemical-controlled recession rate ($\dot{r}_{c,ch}$) in Equation (3).

**Table 3.** The measured erosion of graphite and the C–C composite and their erosion rates.

| | Graphite | | | | C–C |
|---|---|---|---|---|---|
| | **R4340** | **G6520** | **EX60** | **EX70** | **3D** |
| Test time (s) | 120 | 120 | 120 | 120 | 120 |
| Total erosion (mm) | 1.75 | 2.10 | 1.54 | 1.40 | 1.90 |
| Erosion rate (mm/s) | 0.0146 | 0.0175 | 0.0128 | 0.0117 | 0.0158 |

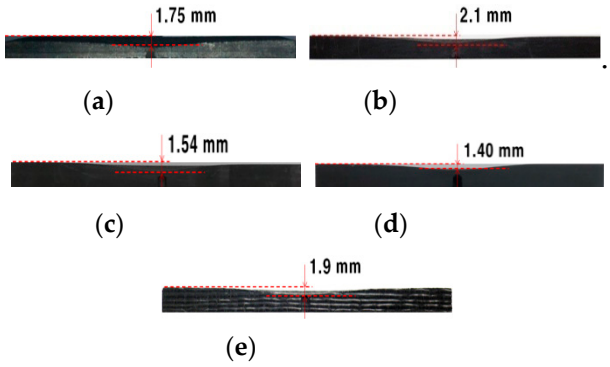


**Figure 9.** Erosion cross section view of (**a**) R4340 (**b**) G6520 (**c**) EX60 (**d**) EX70 (**e**) the 3D C–C composite.

**Table 4.** Calculated thermochemical erosion rate of graphite and the C–C composite.

| | Graphite | | | | C–C |
|---|---|---|---|---|---|
| | **R4340** | **G6520** | **EX60** | **EX70** | **3D** |
| $\dot{r}_{c,\,ch}$ (mm/s) | 0.0305 | 0.0308 | 0.0218 | 0.0251 | 0.0339 |
| $\dot{r}_{c,d}$ (mm/s) | 0.0130 | 0.0131 | 0.0092 | 0.0106 | 0.0145 |
| $\dot{r}_{th}$ (mm/s) | 0.0183 | 0.0184 | 0.0130 | 0.0149 | 0.0203 |
| Error (%) | 25.34 | 5.14 | 1.56 | 27.35 | 28.48 |

The diffusion-controlled recession rate ($\dot{r}_{c,d}$) in Equation (7) is based on values from Table 1. Density, one of main factors influencing the erosion, was obtained from material data sheet and inspection report provided by the manufacturer, the mass fraction of the combustion gas was obtained by NASA CEA [21], and the pressures were measured at 3.6 bar and 5.0 bar. As shown in Table 3, a rather large difference between the measured and predicted erosion rates was observed, and it was found that accurate erosion rate can be predicted only by mechanical erosion considering porosity and shear stress, which is a measure of structural resistance. Porosity is an important factor affecting the erosion resistance of heat-resistant materials and should be considered for erosion prediction.

The mechanical erosion rate ($\dot{r}_m$) was calculated by Equation (10) where the characteristic exhaust velocity of 1008.83 m/s was applied according to the conditions of this experiment, and the porosity was 15% for R4340, 17% for G6520, 14% for EX60, 10% for EX70, and 12% for the 3D C–C composite. Experimental constant (a) was $8.8491 \times 10^{-9}$ derived by curve fitting the experimental data. The mechanical erosion rate was thus calculated by Equation (12), and the rates were computed as 0.01235 mm/s of R4340, 0.01352 mm/s of G6520, 0.01173 mm/s of EX60, 0.00893 mm/s of EX70, and 0.0104 mm/s of the 3D C–C composite.

$$\dot{r}_m = 8.8491 \times 10^{-9} c^* (\log P)^2 \quad (12)$$

The measured and calculated total erosion rates are shown in Table 5 and Figure 10 where the errors between the experimental and predicted values was 7.53% for R4340, 6.29% for G6520, 2.34% for EX60, 4.2% for EX70 and 2.53% for the 3D C–C composite. The overall errors were less than 10%, confirming that the accurate erosion rate can be predicted by considering mechanical erosion.

**Table 5.** The calculated and measured erosion rate of graphite and the C–C composite.

| | Graphite | | | | C–C |
|---|---|---|---|---|---|
| | **R4340** | **G6520** | **EX60** | **EX70** | **3D** |
| Measured erosion rate (mm/s) | 0.0146 | 0.0175 | 0.0128 | 0.0117 | 0.0158 |
| Calculated erosion rate (mm/s) | 0.0157 | 0.0164 | 0.0125 | 0.0122 | 0.0154 |
| Error (%) | 7.53 | 6.29 | 2.34 | 4.27 | 2.53 |

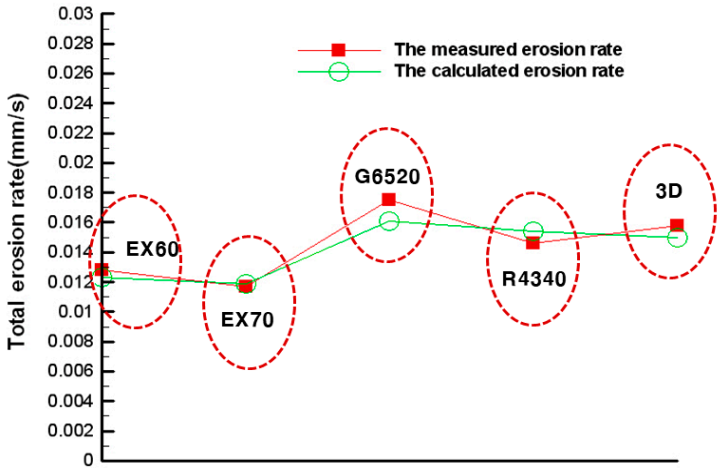


**Figure 10.** Comparison of the measured and calculated erosion rates of graphite and the C–C composite.

The main causes of erosion are thermochemical and mechanical factors. The surface temperature, surface pressure, species concentration and density are the main influences on thermochemical erosion, and porosity [3–5]. Characteristic exhaust velocity and friction are also factors related to mechanical erosion. Figures 11 and 12 show the comparison of erosion rates in terms of density and porosity of graphite. The higher the density, the smaller the erosion rate, and the density of the material has a great effect on the erosion. Additionally, the low porosity slows the erosion rate. When the graphite and C–C composites had a density similar to that of G6520 (1750 kg/m$^3$, 17%) and 3D (1700 kg/m$^3$, 12%), the lower porosity and lighter C–C composites exhibited stronger resistance to erosion.

As the surface temperature increases, and as the concentration of $H_2O$, $CO_2$, and OH increase, the erosion rate increases [8,9]. Therefore, a material with small porosity and high density should be selected or manufactured in order to reduce the erosion of the nozzle heat-resistant material.

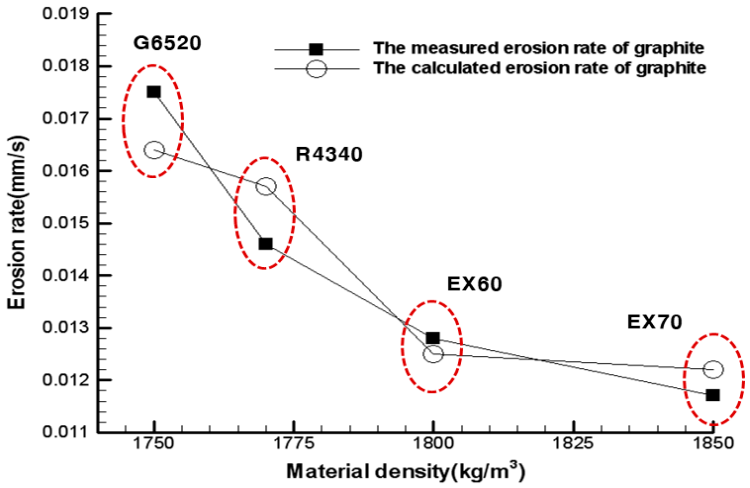


**Figure 11.** Comparison of measured and calculated erosion rates in terms of the density of graphite.

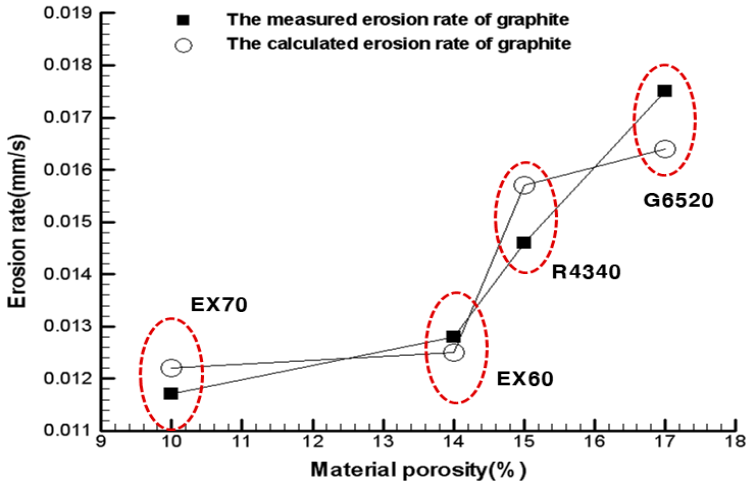


**Figure 12.** Comparison of measured and calculated erosion rates in terms of the porosity of graphite.

## 4. Conclusions

To investigate the thermochemical and mechanical erosion characteristics of graphite and C–C composites used in rocket nozzles, the predicted erosion rate based on the theoretical erosion model was experimentally compared with the amount of erosion. As a result of the analysis, the calculated erosion amount of graphite and the C–C composite material using only the thermochemical erosion model was insufficient due to the large error compared to the experimental results. By considering the estimated erosion rate using the mechanical erosion model with the thermochemical erosion rate, the error between the experimental and predicted values was less than 10%. In addition, in the case of materials with similar properties, C–C composites showed better resistance to erosion than graphite, and surface temperature, surface pressure, species concentration, density, and porosity were major factors influencing erosion. Therefore, these factors should be considered when selecting and manufacturing the nozzle neck material. The results of this analysis can be used as basic data of the air friction erosion of earth re-entrant vehicles.

**Author Contributions:** All authors took part in the discussion of the work described in this paper. All authors read and approved the final manuscript.

**Funding:** This work was supported by the Soonchunhyang University Research Fund.

**Acknowledgments:** The authors thank the editor and anonymous reviewers for their helpful comments and valuable suggestions.

**Conflicts of Interest:** The authors declare no conflict of interest.

## References

1. Hong, Y.S. *Artificial Satellite and Space Lanunch Vehicle*; Cheong-Moon-Gak: Seoul, Korea, 2005; pp. 66–81.
2. Park, I.S.; Oh, I.S.; Joo, H.J. Ablation Characteristics of 4D-Carbon/Carbon Composites. *Korean J. Mater. Res.* **1997**, *7*, 687–693.
3. Kuo, K.K.; Keswani, S.T. A Comprehensive Theoretical Model for Carbon-Carbon Composite Nozzle Recession. *J. Combust. Sci. Technol.* **1985**, *42*, 145–164.
4. Bianchi, D.; Nasuti, F. Thermochemical Erosion Analysis of Carbon-Carbon Nozzles in Solid-Propellant Rocket Motors. In Proceedings of the 46th AIAA/ASME/SAE/ASEE Joint Propulsion Conference & Exhibit, Nashville, TN, USA, 25–28 July 2010.
5. Gowariker, V.R. Mechanical and Chemical Contribution to The Erosion Rates of Graphite Throats in Rocket Motor Nozzle. *J. Spacecr.* **1966**, *3*, 1490–1494. [CrossRef]
6. Acharya, R.; Kuo, K.K. Effect of Pressure and Propellant Composition on Graphite Rocket Nozzle Erosion Rate. *J. Propuls. Power* **2007**, *23*, 1242–1254. [CrossRef]

7. Ham, H.C. The Effect of Pressure and Oxidation Mole Fraction on Ablation Rate of Graphite for Nozzle Throat Insert. *J. Korean Soc. Propuls. Eng.* **2014**, *18*, 8–15. [CrossRef]
8. Ham, H.C. A Study on the Thermal Response Characteristics of Carbon/Carbon Composites for Nozzle Throat Insert. *J. Korean Soc. Propul. Eng.* **2006**, *10*, 30–37.
9. Keswani, S.T.; Andiroglu, E.; Campbell, J.D.; Kuo, K.K. Recession Behavior of Graphitic Nozzles in Simulated Rocket Motors. In Proceedings of the 19th Joint Propulsion Conference/Joint Propulsion Conferences, Seattle, WA, USA, 27–29 June 1983.
10. George, P.S. *Rocket Propulsion Elements*; John Wiley Sons, Inc.: New York, NY, USA, 1992; p. 31.
11. Bianchi, D.; Nasuti, F.; Onofri, M. Thermochemical Erosion Analysis for Carbon-Carbon Rocket Nozzles. In Proceedings of the 45th AIAA/ASME/SAE/ASEE Joint Propulsion Conference & Exhibit, Denver, CO, USA, 2–5 August 2009.
12. Acharya, R.; Kuo, K.K. Numerical Simulation of Graphite Nozzle Erosion with Parametric Analysis. In Proceedings of the 46th AIAA/ASME/SAE/ASEE Joint Propulsion Conference & Exhibit, Nashville, TN, USA, 25–28 July 2010.
13. Kuo, K.K.; Acharya, R. *Applications of Turbulent and Multi-Phase Combustion*; Wiley: Hoboken, NJ, USA, 2012; p. 292.
14. Bianchi, D. Modeling of Ablation Phenomena in Space Applications. Ph.D. Thesis, Sapienza University of Rome, Roma, Italy, 2007.
15. Acharya, R.; Kuo, K.K. Effect of Chamber Pressure & Propellant Composition on Erosion Rate of Graphite Rocket Nozzle. In Proceedings of the 44th AIAA Aerospace Sciences Meeting and Exhibit, Reno, NV, USA, 9–12 January 2006.
16. Joo, H.J.; Kim, Y. A Study of Ablative Behavior on Carbon/Carbon Composites. *Korea Sci. Eng. Found.* **2002**, *1*, 11–14.
17. ASTM. *Standard Test Method for Oxyacetylene Ablation Testing of Thermal Insulation Materials, E285-08*; ASTM International: West Conshohocken, PA, USA, 2015.
18. Winya, N.; Chankapoe, S.; Kiriratnikom, C. Ablation, Mechanical and Thermal Properties of Fiber/Phenolic Matrix Composites. *World Acad. Sci. Eng. Technol.* **2012**, *6*, 556–559.
19. *Chino Corporation, Portable Digital Radiation Thermometer Instructions, INE-374-P10CE*; Chino Corporation: Tokyo, Japan, 2017.
20. National Instruments. *Users Guide and Spec. NI USB-6008/6009*; National Instruments: Austin, TX, USA, 2013.
21. Gordon, S.; McBride, B.J. *Computer Program for Calculation of Complex Chemical Equilibrium Compositions and Applications. Part 1: Analysis*, NASA Lewis Research Center, NASA Reference Publication 1311: Cleveland, OH, USA, 1994.